Study of gas sorption in polymeric membranes from MD&MC simulations

Ioana Cozmuta, Alejandro Strachan, Mario Blanco and William A. Goddard III

ABSTRACT

The barrier properties of membranes for permeability of gases such as O_2, H_2O, N_2, and CO_2 are important for many industrial processes, but there remains inadequate understanding of how to design new improved materials for selective permeability. Partly the problem originates in the difficulty to obtain accurate reproducible experimental data. Simulation methods using first principle predictions have also not been adequately tested. The present work is part of a program initiated at MSC Caltech to improve on the methods to calculate permeability properties of polymeric membranes by focusing first on how to calculate the *sorption* of molecules in a polymeric membrane. Results of molecular dynamics (MD) and Monte Carlo (MC) computer simulation on such polymeric systems as Polypropylene (PP), Polyvinyl alcohol (PVOH), Polyvinyldichloride (PVDC), Polyvinylchloride-trifluoroethylene (PCTFE), and Polyethyleneterephtalate (PET) are discussed. Although oxygen and water solute molecules are of main interest, to validate the calculations against experimental results, the solubilities of nitrogen and carbon dioxide in molten polypropylene are examined. For this last case gas solubilities are calculated for temperatures ranging from 250K to 650K. The magnitudes of the calculated solubilities agree well with experimental results and the trends with temperature are predicted correctly.

1 Introduction

The adsorption of small molecules in polymeric matrices is of great scientific interest for applications ranging from catalysis, to separation technology, to development of new polymeric membranes with improved barrier properties. Of particular interest are polymer materials that serve as barriers with low permeability to gases, vapors, and liquids, especially those that reduce permeability to oxygen gas and water vapor. The large variety of existing polymeric membranes may exhibit barrier properties that are very different with respect to gas and water vapor [12]. Thus, the question that most naturally occurs is what makes a polymeric membrane a good barrier?

To quantify and characterize the barrier properties of a polymer film or membrane, the most frequently measured and reported quantity is the permeability P, by definition written as:

$$P = \frac{(quantity\ of\ permeant)x(film\ thickness)}{(area)x(time)x(pressure\ drop\ across\ membrane)}. \quad \textbf{(1)}$$

This definition, mostly employed by experimentalists, corresponds to a gas permeant at two different pressures on opposite sides of "a mm thick" membrane[1]. A molecular representation corresponding to this definition would result in an extremely large system for which permeability calculations are computationally expensive, if feasible at all.

Alternatively, the permeability of a polymeric membrane is defined as the product between the diffusion coefficient, D, and the solubility coefficient, S, of the penetrant in the bulk polymer:

$$P = D\,S. \qquad (2)$$

The corresponding SI units are cm^2s^{-1} for the diffusion coefficient and cm^3 of gas at STP per volume of polymer (cm^3) and gas pressure (Pa) for the solubility.

Thus, for molecular simulations the permeability may be determined by separately calculating the diffusion (D) and solubility (S) coefficients for the bulk polymer under periodic boundary conditions without explicitly considering the membrane thickness.

It is known [2] that the diffusion coefficient and the solubility of a gas depend on various parameters characterizing the polymeric membrane (chemical structure and morphology), on the physical interactions between the penetrant and barrier material (hydrogen bonds, polar group interactions) and on environmental parameters (temperature, pressure, relative humidity). However, the key scientific interest is to study how the permeability of a certain membrane is related to its structural characteristics and to the solute-polymer interactions.

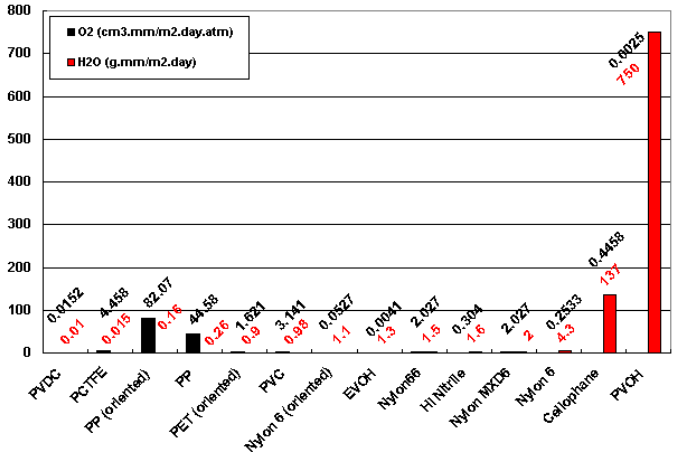

Figure 1: Experimental permeabilities for water vapor and oxygen for various polymeric membranes [12].

A program has been initiated at MSC, Caltech to improve on the methods to estimate permeability properties of polymeric membranes. This method is built upon Molecular Dynamics (MD) simulations [1] of solute molecules diffusing through a bulk polymer to obtain parameters (especially a time scale) for a Monte Carlo (MC) simulation of the diffusion coefficient. The calculated values of the diffusion coefficients and solubilities are then inserted in Eq. 2 to estimate the corresponding permeabilities that are further compared to available experimental data.

[1] A similar expression of permeability can be derived for the permeant being a liquid.

As part of this program, a combined molecular dynamics (MD) and Monte Carlo (MC) methodology described in the present paper is used to calculate solubility properties of polymeric membranes. Although in the present study solubility properties are calculated mainly for oxygen and water, this method could be applied as well for a variety of other solutes.

After a brief introduction, section 2 describes the methods employed to generate and refine atomistic structures of various amorphous polymers. Section 3 discusses a Monte Carlo method to estimate Henry's constant, equivalent to the Grand Canonical method. The precision of the method with respect to various parameters in the numerical calculations is investigated. The selected method to calculate Henry's constant is validated by comparing the calculated solubilities of nitrogen and carbon dioxide in polypropylene with experimental results (section 4) for a range of temperatures. Section 5 discusses the results of the calculations of solubilities for oxygen and water in various selected polymeric systems.

2 Polymer models

Figure 1 summarizes experimentally determined permeability values with respect to water vapor and oxygen for a set of 14 polymers. For both permeants, these values range over several orders of magnitude. Also, membranes that are permeable to oxygen seem to oppose less water permeation and vice versa. For example, polyvinyl alcohol (PVOH) is very good in impeding oxygen but does not block water passage while polypropylene (PP) exhibits the contrary. On the other hand, polyvinylidene chloride (PVDC) is a good barrier for both oxygen and water vapor while polyethylene terephtalate (PET) has average barrier properties for these solutes [12]. For modeling purposes, five polymers out of this set were selected on the basis of being most representative: polyvinyl alcohol (PVOH), polyvinyl dichloride (PVDC), polyvinyl chloride trifluoro-ethylene (PCTFE), polypropylene (PP) and polyethylene terephtalate (PET). The chemical structures of these five polymers are shown in Figure 2.

The Cerius[2] (Accelrys Inc.) amorphous builder module was used to build $n = 10$ samples for each polymer with a unit cell containing four independent molecular chains, each with degree of polymerization D.P. = 20. For the PET sample a D. P. of 5 was used[2]. Also an additional set of n=100 samples was built.

The amorphous builder module requires as input the Rotational Isomeric State (RIS) table that contains information on the conditional probability of key dihedral angles in the chain.

[2] As for PET the number of atoms in the polymeric chain is larger than that of the other polymers, a 5mer instead of a 20mer, having the same number of atoms as the 20mers of PP, PCTFE, PVDC, PVOH was constructed. Due to the presence of chiral centers, for PP and PCTFE syndiotactic samples were built.

The RIS table was determined for each polymer sample (see appendix) by separately minimizing the energy of each representative torsion, with coupling where applicable. The use of the RIS table within this building procedure ensures that polymer samples with nearly optimized geometries are produced, with the proper conformational statistics. The bulk polymer samples are generated initially at low density and are modeled in an infinite periodic unit cell.

The charges on the polymers are from electrostatic potential fits (ESP) to Hartree Fock quantum mechanics determined charges using the 6-31G** basis set. The atomic charges from topologically equivalent atoms were then averaged out. The QM calculations were performed for the polymers trimers rather than monomers to reduce end effects. Furthermore, the charges for the terminal atoms were modified to ensure a zero net charge for the monomer.

The RIS tables and QM determined charges for each of the five polymers selected for the present study are summarized in the Appendix.

For the MD runs, two versions of the Dreiding [8] force field were used, one for non-periodic vacuum calculations (file *dreidii-exp6-direct.par*) and the second for condensed phase periodic systems (*dreidii-exp6-ewald.par*).

For each of the *n* samples generated for each polymer, the equilibrium unit cell volumes and densities are obtained by a series of compression/expansion and heating/cooling

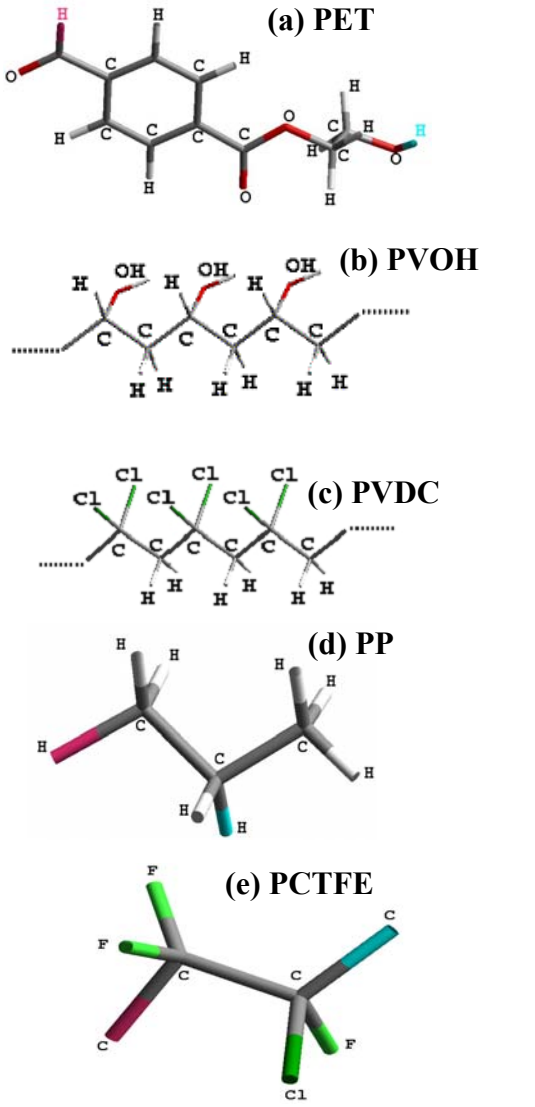

Figure 2: Chemical structures of studied polymers.

cycles according to the procedure described below.

1. The polymer sample is built in a cubic cell with a target density of 40% of the expected density, ρ_{exp} (usually chosen as the experimental value) using the RIS MC technique described above.
2. The structure is energy minimized holding the unit cell parameters fix.

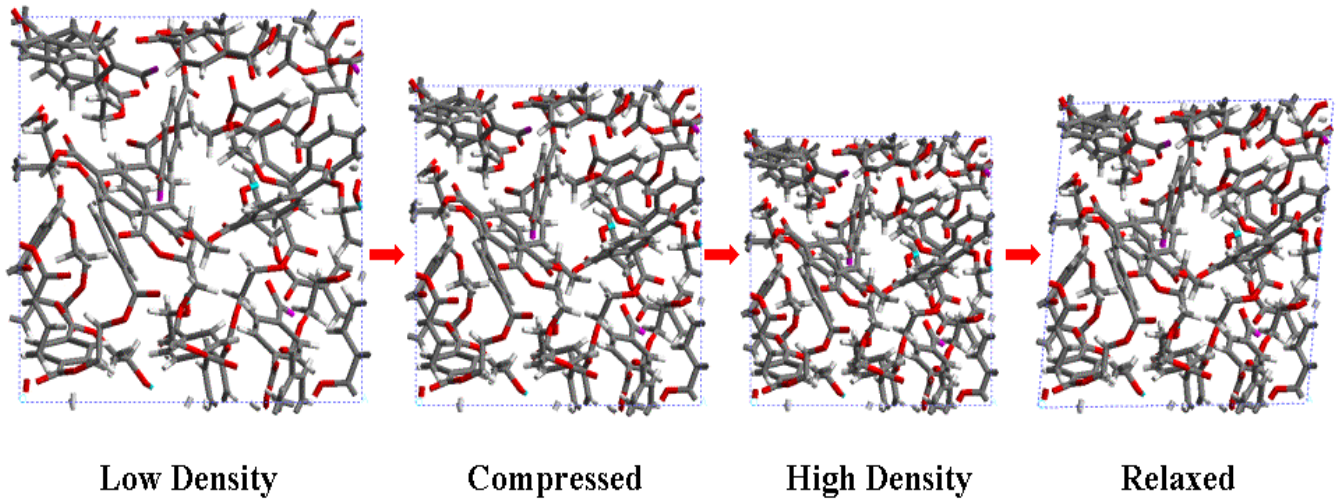

Figure 3. Anneal dynamics protocol schematized for the PET sample. The target density is the experimental density for amorphous PET, ρ_{exp}=1.3 g/cc. The low-density state corresponds to 0.4ρ_{exp}, the compressed state to 0.8ρ_{exp} and the high-density state to 1.2ρ_{exp}.

Table 1. Summary of information from the anneal dynamics cycle: Degree of Polymerization (D.P.), cohesive-energy density (CED), solubility, volume, end-to-end distance, radius of gyration, and energy per mol of monomer for the investigated polymer samples. The average density values are listed in Table 2 together with experimental values. The experimental range for the solubility parameter is also given in this table [4, 16]. The number of samples (n) is 10 or 100 for the case of PET.

Polymer (n)	D.P.	CED	Solubility parameter		Volume	$R_{end-end}$	R_g	E_b
-	-	cal/cc	$(cal/cc)^{1/2}$		$Å^3$/UC	Å	Å	(kcal/mol of monomer)
			Calculated	Experimental				
PET (10)	20	(-142.62±10.71)	(11.93±0.45)	[9.7-10.7]	(5076.21±92.26)	(14.90±0.84)	(7.04±0.39)	(-21.8±2.3)
PET(100)	20	(-151.49±11.40)	(12.3±0.46)	[9.7-10.7]	(5028.11±124.00)	(14.93±1.97)	(7.02±0.36)	(-22.9±0.7)
PVOH (10)	80	(-262.75±16.38)	(16.20±0.51)	[12.7-14.2]	(4856.83±89.12)	(25.2±3.49)	(9.52±0.61)	(-73.4±0.3)
PVDC (10)	80	(-71.47±10.07)	(8.44±0.59)	[9.3-10.8]	(8558.86±293.06)	(13.83±2.88)	(7.25±0.56)	(-2.1±0.2)
PCTFE (10)	80	(-46.14±5.47)	(6.78±0.40)	[7.2-7.9]	(8658.64±334.90)	(17.65±2.53)	(7.91±0.48)	(-13.3±0.3)
PP (10)	80	(-48.00±5.04)	(6.91±0.36)	[7.7-9.4]	(6896.35±188.66)	(14.29±2.29)	(6.96±0.37)	(-107.8±0.2)

3. At each density the structure is again energy minimized for 500 steps followed by 0.5 ps of NVT MD at 500K.
4. The system is compressed in four steps (0.6, 0.8, 1.0, 1.2 ρ_{exp}) to achieve a final density of 1.2 ρ_{exp}.
5. The system is allowed to relax (expand) to a final density ρ_{exp} in four steps (1.15, 1.1, 1.05, 1.0 ρ_{exp}).
6. At each density, the structure is energy minimized for 500 steps followed by 0.5 ps of NVT MD at 500K.
7. The final structure resulting from step 6 is energy minimized for 500 steps and equilibrated using NPT MD for 10 ps at 298K. This leads finally to a relaxed state with density close to ρ_{exp}.

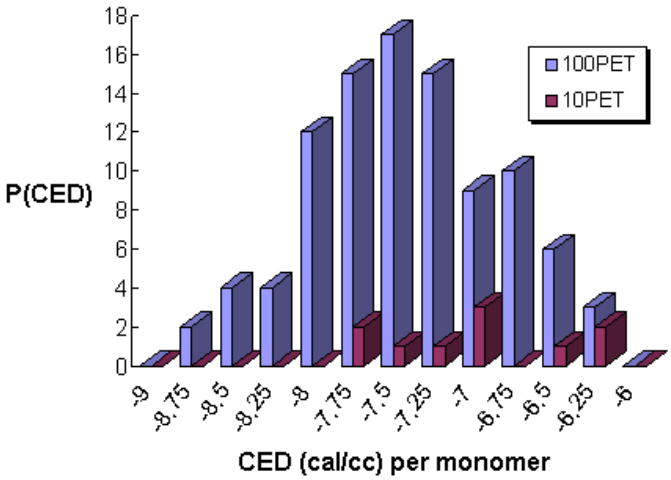

Figure 4a. Probability distribution of the *cohesive energy density* per monomer (the CED values from Table 1 are divided by the D.P.) for the PET polymer for two sets of samples, *n*=10 and *n*=100. The Boltzmann averages are –7.5 cal/cc and –8.1 cal/cc, respectively.

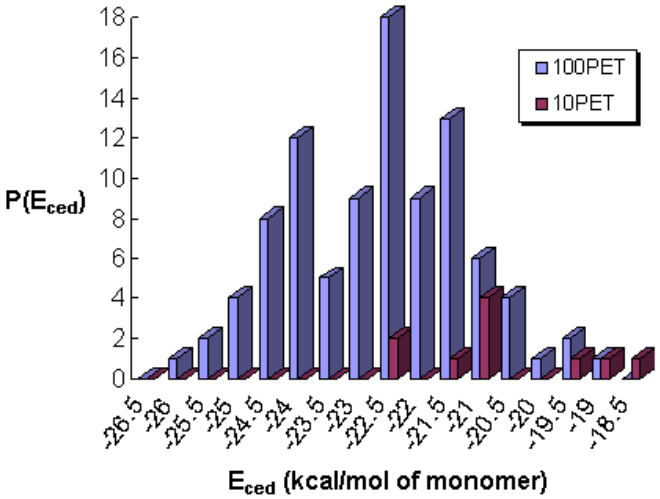

Figure 4b. Probability distribution of the *cohesive energy* per monomer (the CED values from Table 1 are multiplied by the volume of each sample and divided by the D.P.) for the PET polymer for two sets of samples, *n*=10 and *n*=100. The Boltzmann averages are –22.4 kcal/mol and –25.3 kcal/mol, respectively.

At the end of the anneal dynamics cycle, several physical and chemical properties (density, solubility parameters, end-to-end distance, and radius of gyration) are calculated as averages over the number *n* of generated samples. The cohesive energy density (CED) is also calculated during this cycle as the difference between the total energy of the bulk system (all terms in the energy expression) and the sum of the gas phase energies for each of the four polymer strands composing the unit cell divided by the volume of the unit cell. The Hildebrand solubility parameters are calculated using the standard definition [13]. The above procedure to generate polymeric samples will be further referred as the CED procedure and it is in more detail described elsewhere [13].

The average values and the standard deviations reported in Table 1 for the five investigated polymers are calculated at the 95% confidence limit (2σ on each side of the average). The last column in Table 1 is the total energy per monomer unit averaged over the 10 ps NPT dynamics at 298K (step 7) by sampling every 0.5 ps.

To determine whether the sample set of *n*=10 is statistically adequate, the CED procedure is repeated to generate an additional set of *n*=100 PET samples. Three types of energies are calculated and compared for the two sets of PET samples:

- The CED per monomer, *CED (cal/cc)*, by dividing the values of the CED (Table 1) with the D.P. value (Figure 4a).

- The energy per monomer, E_{ced} *(kcal/mol)*, by multiplying the values of the CED with the volumes of each sample and dividing by the D.P. (Figure 4b).
- The energy per monomer, *E (kcal/mol)*, by calculating the final total single point energy of each minimized sample and dividing the value by the D.P. (Figure 4c).

The probability distributions of these energies for the *n*=10 and *n*=100 sets are shown in Figures 4a-4c and the average and standard deviations summarized in Table 2.

Additionally, the Boltzmann average is also calculated from:

$$\langle E \rangle = \frac{\sum E * \exp\left(-\frac{E}{k_B T}\right)}{\sum \exp\left(-\frac{E}{k_B T}\right)} \qquad \textbf{(3)}$$

The Boltzmann averages calculated for the cohesive energy density values (per monomer) for the two sample sets have relatively close values, –7.5 cal/cc (*n*=10) and –8.1 cal/cc (*n*=100). A somewhat larger difference is observed when comparing the Boltzmann averages calculated for the E_{ced} data; the –22.4 kcal/mol value for the *n*=10 set being less negative than the –25.3 kcal/mol value for the *n*=100 set. These values, correlated with the probability distributions in Figure 4a and Figure 4b, suggest that by generating a smaller set of samples (*n*=10 versus *n*=100) the sampling may be biased towards configurations with higher energies. When the two sets of PET samples generated with the CED procedure are additionally minimized, the Boltzmann averages calculated for the final total minimized energies, *E*, agree very well, 44.8 kcal/mol (*n*=10) versus 44.6 kcal/mol (*n*=100). Also the probability distribution for these energies seems to indicate that the sampled configurations in the small set (*n*=10) can be considered representative of the larger (*n*=100) set.

Table 2. Average and standard deviation of energy values for PET for the *n*=10 and *n*=100 sets of samples.

No. PET	CED	E_{ced}	E
	cal/cc	kcal/mol	kcal/mol
10	(-7.1±0.5)	(-20.9±1.3)	(45.2±0.5)
100	(-7.6±0.6)	(-22.9±1.4)	(45.4±0.7)

The accuracy with which the sample mean estimates the population mean is given by the standard error, which is typically calculated as the sample standard deviation divided by the square root of the number of points in the sample less one. When comparing average and standard deviation values for the three types of calculated energies and for the two sets of PET samples (Table 2), the variation lays within 10%, value that can be considered a reasonable threshold.

Thus the *n*=10 set seems to provide a sufficiently accurate representation of the distribution obtained with the larger *n*=100 set by preserving key properties of the polymer samples. Consequently, for the other polymers

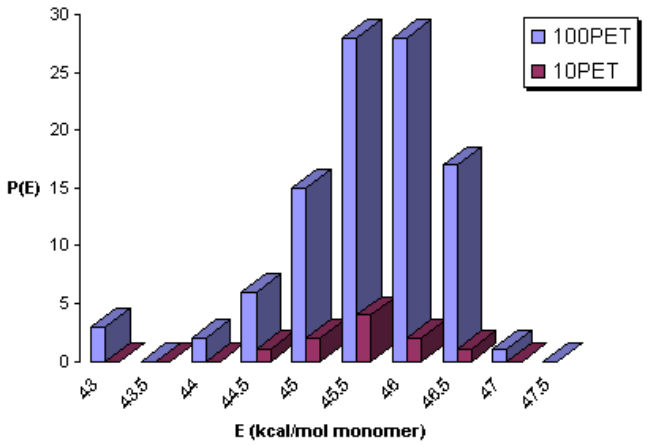

Figure 4c. Probability distribution of the *single point energy* per mol of monomer (D.P.) for the PET polymer for two sets of samples: *n*= 10 and *n*=100. The Boltzmann averages are 44.8 kcal/mol and 44.6 kcal/mol, respectively.

selected for our permeability study (PP, PVDC, PVOH, PCTFE) the sample generation via the CED procedure was limited to the *n*=10 set.

However, for the purpose of solubility calculations one sample out of the generated *n*=10 set is selected based on the criterion that it should best represent the average density and CED of the ten samples. For this "average" sample an additional 150 ps of NPT dynamics (constant number of particles, pressure and temperature) at a temperature of 298K and pressure of 1 atm = $1.0132*10^{-4}$ GPa is run. During the NPT dynamics the Nose-Hoover thermostat and the Parrinello-Rahman barostat are used. The equilibrated part (last 100 ps) of the NPT-MD generated trajectories is further used for solubility calculations.

Table 3 shows the experimental densities reported for the amorphous polymers [4], ρ_{exp}, the annealing densities (averaged over the dynamics at 298K for all *n* samples), ρ_{anneal}, and the minimized density (from all *n* samples), ρ_{min}. For comparison, the densities corresponding to the lowest cohesive energy density, ρ_{CED}, and the average density from the NPT dynamics, ρ_{NPT}, for the single selected sample from the *n* cases are also indicated.

These values show that the CED procedure leads to densities that are too low by ~ 6% to 15% when experimental densities (ρ_{exp}) are compared to the average over all *n* generated samples (ρ_{anneal}). The densities of the lowest CED sample (ρ_{CED}) are smaller by only 2% to 9 % compared to the experimental values.

Table 3. Comparison of experimental densities, ρ_{exp}, [4, 16] with the densities from annealing, ρ_{anneal}, additional minimization, ρ_{min}, the density corresponding to the lowest CED sample, ρ_{CED}, and one-sample NPT dynamics-average, ρ_{NPT}.

Polymer	ρ_{exp}	ρ_{anneal}	ρ_{min}	ρ_{lCED}	ρ_{NPT}
	g/cc	g/cc	g/cc	g/cc	g/cc
PET10	1.34	(1.26±0.02)	(1.31±0.02)	1.29	(1.29±0.03)
PET100	1.34	(1.27±0.03)	(1.32±0.03)	1.31	n.a.
PVOH	1.29	(1.21±0.02)	(1.21±0.03)	1.25	(1.24±0.03)
PVDC	1.66	(1.51±0.05)	(1.57±0.03)	1.62	(1.64±0.03)
PCTFE	2.1	(1.79±0.07)	(1.79±0.07)	1.90	(1.77±0.05)
PP	0.86	(0.81±0.03)	(0.82±0.02)	0.86	(0.76±0.03)

In general, an underestimate in the densities of the samples generated for MD is to be expected as industrial grade polymers typically have D.P. well over 1,000, much larger than the low molecular weights polymers (D.P 20) modeled in this study. Long chains are however impractical to model due to the long simulation time scales one would require.

3 Methodology to calculate solubility constants

Solubility represents the ability of a substance to dissolve into another. Its value expresses the maximum amount of solute that will dissolve in a given amount of solvent. For gases in polymers, the solubility *S* describes the concentration *C* of the gas inside a polymer at equilibrium with the gas at partial pressure *p* and is described by the dual-mode theory [18]:

$$C = k_H p + C_\infty \frac{bp}{1+bp} \qquad (4)$$

This equation accounts for two distinct mechanisms of sorption: the first term corresponds to Henry's law, proportional to *p*, while the second term represents a Langmuir-type isotherm with c_∞ the saturation concentration of the gas and *b* the ratio of gas molecules absorption/desorption rates.

For ideal dilute solutions (real solutions at low concentrations), the case of gases in rubbery polymers, one may ignore the Langmuir part in Eq. 4. For such rubbery polymers, Henry's law is obeyed up to pressures of several hundred atmospheres [14, 18]. The relation between solubility and Henry's constant (expressed in standard units of Pa^{-1}) can be derived by assuming that the gas exhibits ideal-gas behavior both at *STP* conditions (T_0=273.15 K, p_0=1 atm) and at the temperature *T* of the measurements (i.e. $V/V(STP)=T/273.15$ K):

$$S = k_H \frac{T}{273.15K} \qquad \textbf{(5)}$$

In computer simulations, Henry's constant is usually calculated via Monte Carlo statistical mechanics methods [3,6]. There are two equivalent modalities to perform such calculations. The first requires the evaluation of the simulation-cell loading at several fixed pressure (grand canonical ensemble). Henry's constant, k_H, is then calculated as the simulation-cell loading, *C* divided by the sorbate pressure, *p* in the limit of zero pressure:

$$k_H = \lim_{p\to 0} \frac{C}{p} \qquad (6)$$

Bezus [7] proved that Henry's constant may be computed from configuration integrals corresponding to different positions ***r*** and orientations Θ of the solute molecule inside the cavities of the polymer matrix:

$$k_H = \frac{1}{k_B T} \int_{cell} dr \int \frac{d\Theta}{8\pi^2} \exp^{\frac{-U(r,\Theta)}{k_B T}} \qquad \textbf{(7)}$$

In practice, these cavities are partitioned into small cells and the energies of interaction, U(r,Θ) are calculated at the centers of these cells. It is assumed that at any point inside a given cell the corresponding contribution to the total energy of interaction is equal to the value calculated for the center of the cell. Thus the integral in Equation 7 becomes the finite sum:

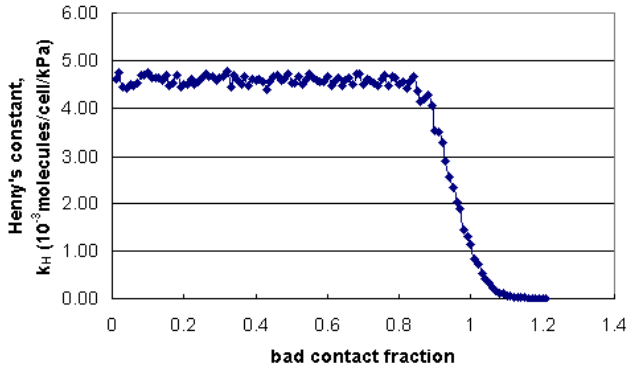

Figure 5. Henry's constant, k_H, versus the bad contact fraction, *f*. A bad contact fraction occurs when two atoms approach within a defined fraction *f* of the sum of their van der Waals radii.

$$k_H \approx \frac{Vcell}{k_B T}\frac{1}{N}\sum_i e^{\frac{-U(r_i,\Theta_i)}{k_B T}} \qquad \textbf{(8)}$$

with V_{cell} the volume of the unit cell and N the adjustable number of steps in the simulation. The positions (r_i) and orientations (Θ_i) are chosen at random [7]. This procedure is implemented in Cerius^2 (Accelrys Inc.) under the choice of Henry's constant ensemble [5] and requires as input the model of the polymer framework and a model of the sorbate molecule of interest. The program will then generate N random, positions and orientations for the sorbate molecule. For all accepted configurations the solute-matrix and the solute-solute (images) interaction energies are calculated and added to the sum in Equation 7. Henry's constant is returned at the end of the calculation in units of **molecules/unit cell/kPa.** Throughout this paper we will report the values of Henry's constant in cm^3(*STP*)cm^{-3}atm^{-1}, since the experimental data are usually expressed in terms of volume of gas at standard temperature and pressure (*STP*) adsorbed in a certain volume of polymeric material at the pressure of interest, *p*.

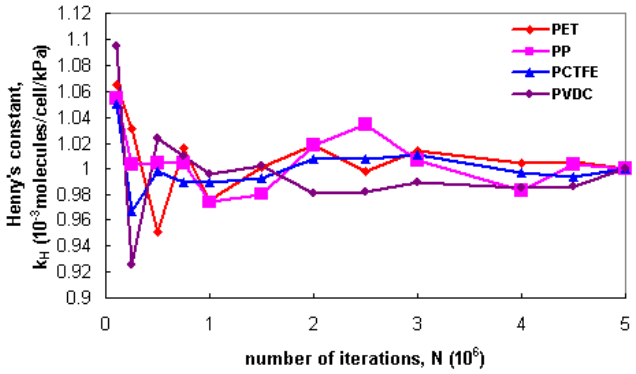

Figure 6. Calculated values for Henry's constant, k_H, as function of the number of terms, *N*, in the sum of Equation 8. All k_H values are normalized to the converged value obtained for *N*=5millions iterations.

Accepted configurations depend upon a bad contact fraction parameter set by the user. Before performing an energy calculation, the program checks for bad contacts to identify and reject such high-energy configurations (that would give negligible contributions to the sum) to save calculation time. A bad contact occurs when two atoms approach within a defined fraction *f* of the sum of their van der Waals radii. In the present calculations, a value of 0.5 is chosen for this fraction.

Figure 5 shows the variation of the solubility coefficient (Henry's constant) as a function of the bad contact fraction *f* calculated for one frame of the PET sample. If the value of *f* is too large, many bad contacts will be found, the calculation will be fast but inaccurate. On the other hand, if *f* is too small, too many high-energy configurations are accepted, slowing

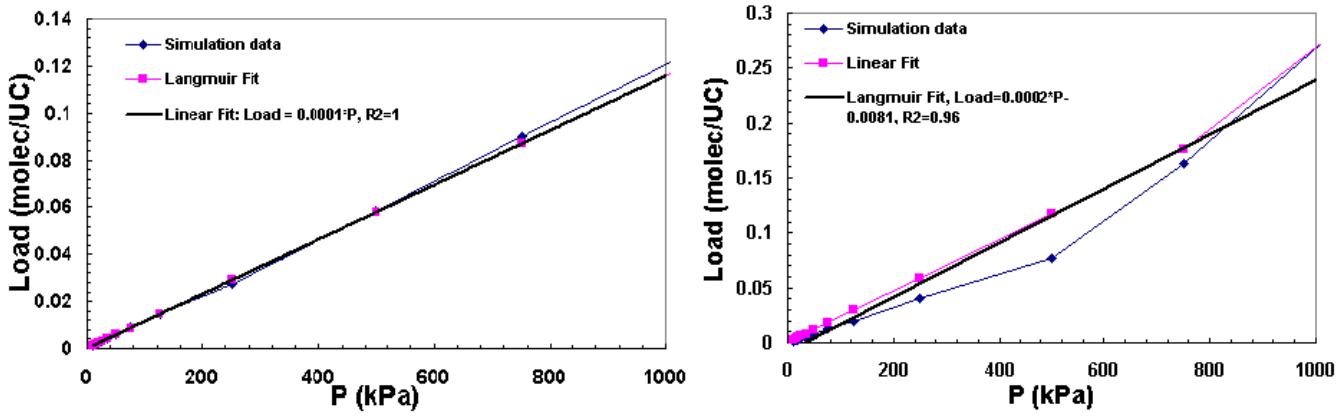

Figure 7. Concentration versus pressure calculation (Grand Canonical ensemble) for the PET sample with H_2O (left) and O_2 (rigth). Equation 4 is then fit through the data points (Langmuir and linear). The calculated fit parameters are k_H =1.16*10^{-4}, b=0.99, c_∞=1.74*10^{-7} for water and k_H =2.35*10^{-4}, b=0.05, c_∞=0.05 for oxygen.

down the calculation without correspondingly increasing the accuracy.

Another adjustable setting in the numerical calculation of Henry's constant is the number of iterations N (the number of terms in the sum of Equation 8). Calculations were carried out for the PET, PP, PCTFE, PVDC polymer samples to check how the precision in Henry's constant determination depends on the number of iterations, N. N was varied from 150,000 to $5\cdot10^6$ steps; for each N, the values of k_H was normalized to the k_H value calculated for N=$5\cdot10^6$. Figure 6 shows that N=$1.5\cdot10^6$ steps is sufficient to obtain a well-converged value of k_H (within 4%) while also convenient from the point of view of computational time (that in principle scales with N). If not otherwise specified, we used the value of $1.5\cdot10^6$ steps for N throughout this paper.

Usually, Henry's constant calculations are performed on rigid frameworks (zeolites, alumino-phosphates, etc.) with micro porous structure that does not change significantly during dynamics simulations. However, for polymeric systems it was observed that the dynamics of the polymer matrix introduces important structural modifications (distribution of voids and channels, destruction of existing voids and generation of new ones). Because the existing free volume and its distribution inside the host matrix influences both diffusion and sorption, Henry's constant is calculated as the average over a selected number of frames (every 0.5 ps) in the equilibrated part (usually 50-150ps) of each MD trajectory. For statistical purposes, a confidence interval rather than an average value is calculated for Henry's constant according to a two-tailed test and a 95% confidence level:

$$\bar{x} - t_{\alpha,n-1}\frac{s}{\sqrt{n}} < \mu \le \bar{x} + t_{\alpha,n-1}\frac{s}{\sqrt{n}} \qquad (9)$$

In Eq. 9, $t_{\alpha,n-1}$ is the value of the standard normal variable that puts $\alpha/2$ percent in each tail of the distribution, μ is the population mean, n the sample size, $\bar{x}$ the sample mean and $\frac{s}{\sqrt{n}}$ the standard error for $\bar{x}$. This procedure is further referred to as the "Henry's constant ensemble" method.

The Dreiding force field [8] was used to evaluate the energy expression in the Henry's constant ensemble calculations.

Table 4. Values of k_H (molecules/cell/kPa) calculated from the Grand Canonical (GC) and Henry's constant (HC) ensembles. Equation 4 was used to fit the concentration versus pressure data via a Langmuir (both terms) or linear (first term only) expression. The R^2 values for the fit of the GC ensemble data are 0.96 for oxygen and 1 for water. Eq. 8 was used for the HC calculations.

PET	GC			HC
	k_H	c_∞	b	k_H
$+O_2$				
-Langmuir	$2.35*10^{-4}$	0.05	0.05	
-Linear	$2.35*10^{-4}$	0	0	$2.9*10^{-4}$
$+H_2O$				
-Langmuir	$1.16*10^{-4}$	0	0.99	
-Linear	$1.16*10^{-4}$	0	0	$1.0*10^{-4}$

This Cerius^2 (Accelrys Inc.) procedure employs the minimum image convention to calculate the van der Waals component of the energy and the Ewald summation method for the Coulomb interactions. However, the latter can be turned off for cases when the solute molecule is not charged (e.g., oxygen, nitrogen) to save computation time. The default non-bond cut-off is initially 8.5Å and is automatically optimized during the calculation to ensure solution consistency [5].

Agreement of the k_H predictions given by the Grand Canonical (Eq. 4) and Henry's constant (Eq. 8) ensembles was checked. Via the GC ensemble, the solute concentration (cell load) for oxygen and water was calculated for the PET matrix for a range of pressures between 0.01 atm and 10 atm (Figure 7). Equation 4 was then fit through the data points to obtain k_H in the limit of zero pressure. The calculated Langmuir parameters, b and c_∞ are both essentially zero (Table 4). The GC ensemble fit values of k_H are compared with the results from Henry's constant (HC) ensemble in Table 4.

The k_H values calculated with the two ensembles agree within 20%. Since the experimental data do not agree better than 10% and since the Henry's constant ensemble calculation is about 10 times faster than GC, we chose to use the Henry's constant ensemble for all our further calculations.

The precision of the k_H procedure was also tested by repeating (three times) the calculation for exactly the same configuration of each of the polymers. The results show that all the calculated values are repeatable within 5%.

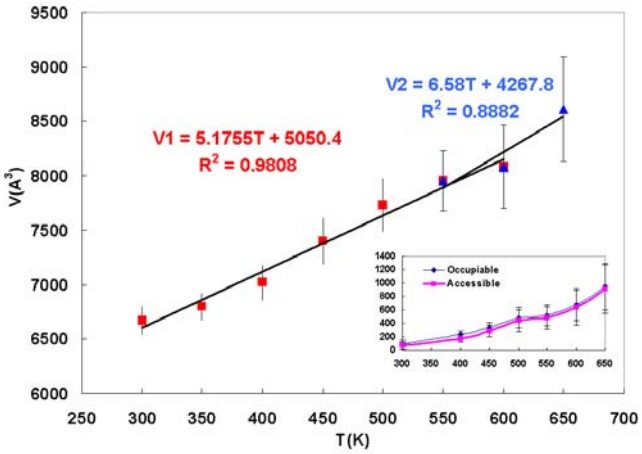

Figure 8: Temperature dependence of the MD-averaged unit cell total volume of PP. The inset represents the temperature dependence of the occupiable and accessible volumes.

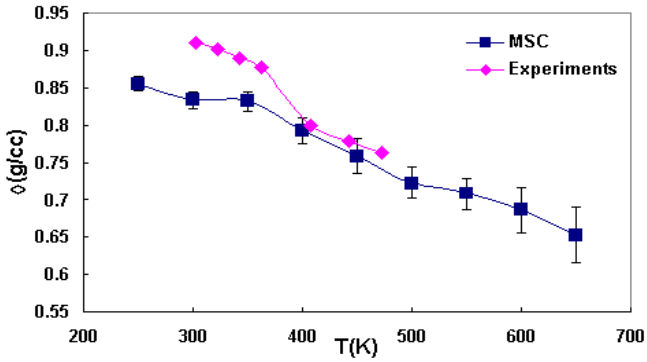

Figure 9: Temperature variation of PP density from MD simulations (squares). For comparison, experimental data (diamonds) are also shown [15].

4 Validation

Accurate experimental values for solubilities in polymeric systems are quite rare in literature, especially at elevated pressures and temperatures. The present study is validated by comparing with data from other literature studies (experimental and calculations) Henry's constant temperature dependence of nitrogen (N_2) and carbon dioxide (CO_2) in polypropylene (PP). The temperature dependence of some of the polymer's matrix properties (compressibility, bulk modulus and thermal expansion) as calculated from MD simulations are first tested.

4.1 Compressibility and thermal expansion coefficients

The MD average of the total, occupiable and available volume (calculated in Cerius^2) shows a linear increase with temperature (Figure 8). However, both graphs exhibit a discontinuity between 450 K and 550 K approximately corresponding to the melting regime of PP.

Additionally, Figure 9 shows the temperature variation of the (syndiotactic) PP density. Experimental densities are available for isotactic PP for temperatures below melting, between 300 K and 473 K [15]. The agreement between calculated and experimental densities is again better for temperatures above the melting point.

From the temperature dependence of the average volume/density, a value of 577 K is predicted from our calculations as the melting temperature of PP. This value is determined from the equality of the linear fits of the data points below and above 500 K (Figure 8).

The *isothermal compressibility*, α (GPa^{-1}), is calculated from the volume fluctuations during MD according to:

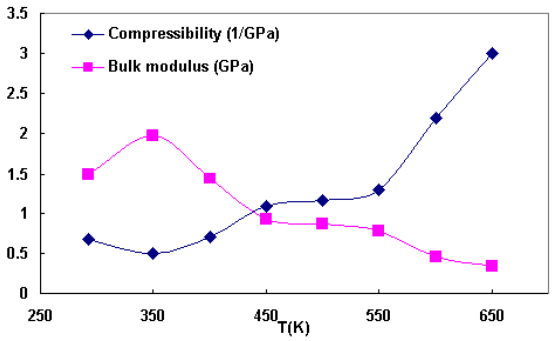

Figure 10: Temperature variation of compressibility, α, and bulk modulus, β, for PP.

$$\alpha = \frac{\langle V^2 \rangle - \langle V \rangle^2}{\langle V \rangle k_B T} \qquad (11)$$

with <> the notation for ensemble averaging, V the total unit cell volume, k_B Boltzmann's constant (=1.38·10^{-23} JK^{-1}) and T (K) the absolute temperature. By definition, *the bulk modulus*, β (GPa), is calculated as the inverse of the isothermal compressibility, α.

The *thermal expansion coefficient*, α_T (K^{-1}), is calculated at each temperature from the linear fit of the volume versus temperature as the slope of V (T) divided by the average MD volume corresponding to temperature T.

Experimental compressibility data is available for melted PP. Table 5 shows that for temperatures between 450K and 550K the isothermal compressibility values calculated in the present study follow the same trend as the experimental data although underestimated by about 15-30%.

Experimental values for the thermal expansion coefficient are available for a broad

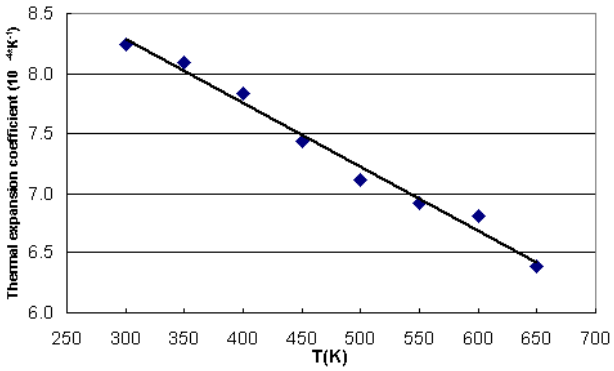

Figure 11: Temperature variation of the thermal expansion coefficient, α_T, of PP.

range of temperatures whereas compressibility data is available only for melted PP. The variation of the thermal expansion coefficient with temperature is shown in Figure 11. The agreement is good for temperatures above 450K (above T_{melt}, 10% high), but the predicted values (Table 6) are high by a factor of 8 near the glass temperature (280K).

Table 5. Coefficient of isothermal compressibility, α(GPa^{-1}), for PP.

T(K)	experiment [4]	present study
453	1.27	1.08(450K)
493	1.5	1.16 (500K)
533	1.78	1.29 (550K)

Table 6. Coefficient of linear thermal expansion and of thermal expansion (melt), α_T (K^{-1}) for PP.

T(K)	experiment [4]	present study
243-273	6.5e-5	
273-303	1.1e-4	8.24e-4
303-330	1.4e-4	8.09e-4
448-573	6.6e-4	7.43e-4 to 6.81e-4
453-503	6.7e-4	

Actually it is more accurate to describe the melting of a polymer as a process that takes place over a range of temperatures, depending on many factors (i.e., molecular weight, chain

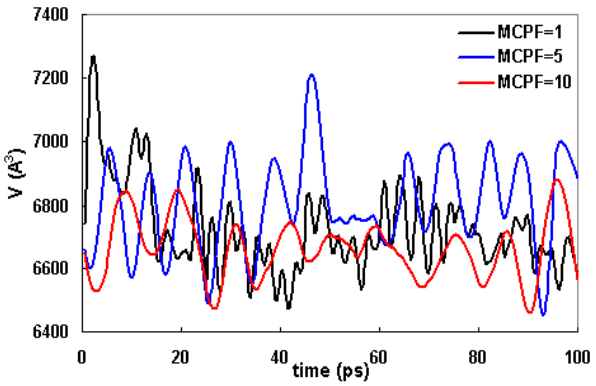

Figure 12. Time variation of unit cell volume for PP at 300K as function of the MCPF used in dynamics (150 ps NPT).

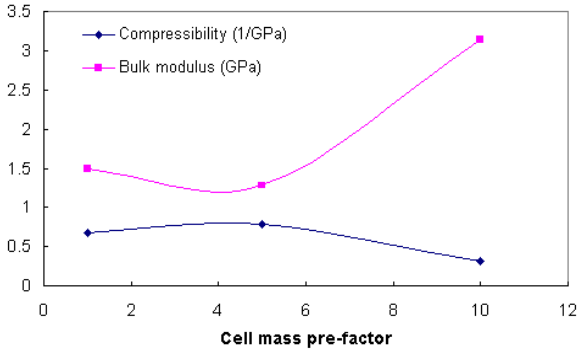

Figure 13. Dependence of compressibility and bulk modulus on the value (1, 5 and 10) of the cell mass pre-factor (MCPF) set in the NPT dynamics calculation at 300K for PP

stiffness, degree of branching, etc.). The data points in Figure 8 - Figure 11 indicate that the PP melting process starts somewhere between 400 K and 450 K and is completed around 550 K.

Depending on the extrapolation technique used to calculate melting temperatures from experimental data a range between 415K and 477 K was determined for syndiotactic PP for the equilibrium melting temperature [17]. The 477 K value corresponds to 100% syndiotactic PP. For comparison, for isotactic PP the melting temperature ranges from 398 K to 439 K.

The values predicted in the present study are in good agreement with the experimental ranges considering that our modeled polymer has a lower molecular weight (At relatively low molecular weights it was observed that increasing the mass or chain length results in raising the melting temperature).

4.2 Mass cell pre-factor coefficient

In the Rahman-Parrinello approach (the barostat used in the NPT calculations to preserve constant pressure in the system) a user-defined mass-like parameter corresponding to the volume dynamical variable is used to calculate the kinetic energy of the cell. This represents actually the piston mass and is considered in the dynamics as a mass cell pre-factor (MCPF) controlling the heat flow rate. A value of 1 for MCPF was used so far in our calculations. Generally this value should be chosen such that the fluctuations in the volume are much slower than in the temperature. In addition the volume properties should be calculated over a large number (~20) of these long-term fluctuations.

To verify the influence of the MCPF on the dynamics and the calculated k_H values, additional 100 ps of NPT dynamics at 300K were run with values of the mass cell pre-factor of 5 and 10,

respectively. Figure 12 shows the time variation during dynamics of the total unit cell volume for the three values of the MCPF. With increasing piston mass (larger MCPF values), the volume space is less explored and the volume fluctuations decrease in amplitude and periodicity. Too small values selected for MCPF result in fast motion of the cell vectors but could induce artificial periodic motions of the cell and may not allow enough time for equilibration. Larger values of MCPF mean a heavy, slow fluctuating cell (for infinite value of MCPF constant-volume dynamics should be obtained) thus, requiring longer dynamics runs. Here it appears that the 100 ps of sampling is sufficient for MCPF=1 and 5, but perhaps not for MCPF=10.

Consistent with the volume fluctuations, the compressibility is also not well represented for large values of the MCPF (Figure 13).

The time variation of k_H calculated using the Henry's constant ensemble from the NPT-MD simulations at 300K for each of the three values of MCPF (1, 5 and 10, respectively) is shown in Figure 14. The limits for a 95% confidence interval of k_H and the average total unit cell volumes are summarized in Table 7.

Both data in Figure 14 and Table 7 seem to indicate that it would be beneficial for the accuracy of the calculated k_H values to allow a slower exploration of the volume (MCPF=10). Indeed, the time fluctuation and the limits of the

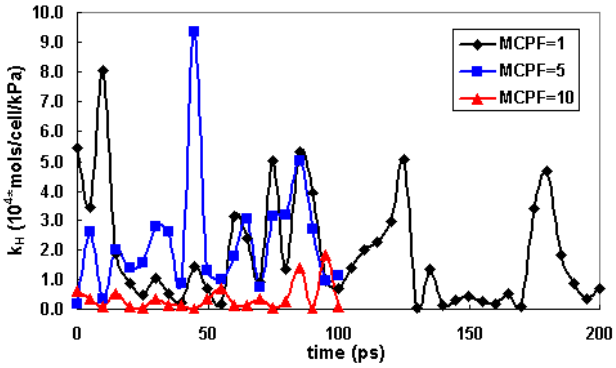

Figure 14. Time variation of Henry's constant, k_H, calculated from NPT dynamics for PP at 300K using three values for the mass cell pre-factor, MCPF, in the Rahman-Parrinello barostat.

confidence interval calculated for k_H for MCPF=10 are smaller than for MCPF=5 and MCPF=1. However, by exploring less the volume space fewer polymer configurations are also sampled and representative contributions may be lost. Using a larger value for MCPF would mainly result in increasing the simulation time.

Table 7. Confidence intervals of k_H calculated for N_2 in PP at 300K corresponding to three values of the mass cell pre-factor (MCPF) in the Rahman-Parrinello barostat. The averages of the total unit cell volume, V, over the MD simulation times, t, are also indicated.

MCPF	t (ps)	V (Å^3)	k_H (cc^3/kg/MPa)
1	200	6672±135	(838< k_H ≤1590)
5	100	6807±149	(879< k_H ≤2010)
10	100	6660±94	(99< k_H ≤368)

This analysis proves that the choice of a MCPF value of 1 is optimal from the point of view of exploration of the volume domain and the required simulation time.

4.3 Temperature dependence of k_H

The study by Durrill & Griskey [9] contains data on measured solubilities and diffusivities of various gases in molten or thermally softened polymers. The experimental procedure involves saturation of the polymer matrix with the gas at low pressure. As a response to the initial quick increase in pressure, the solute starts permeating the polymer. The pressure drop rate is then recorded. From the pressure versus time curves, by repeating this procedure at various pressures, the gas solubilities/Henry's constant were calculated. The precision of the experimental data claimed by the authors is about 8%. Table 8 contains Henry's constant values from this study determined at 461K.

Using the Sanchez-Lacombe equation of state, Sato *et al.* [10] report the following linear relationship between Henry's constant (k_H) and temperature:

$$for\ N_2: \quad \ln k_H = 8.407 - 20.39 * \left(\frac{T_c}{T}\right)^2 \qquad (10)$$

$$for\ CO_2: \quad \ln k_H = 6.255 + 3.706 * \left(\frac{T_c}{T}\right)^2$$

with T_c(K) the critical temperature of the gas[3] and T(K) the actual temperature of the system. The Sanchez-Lacombe equation of state predicts the swelling of the polymer matrix in the presence of a gas/solute, given a certain pressure. The Sato *et al.* values in Table 8 are calculated from Eq.10 at T=461K.

For PP a 453.2K MD trajectory was initially available and the confidence interval for k_H was estimated for N_2 and CO_2 at this temperature using the Henry's constant ensemble method (Table 8).

With respect to the experimental data [9] the Sanchez Lacombe EOS overestimates the CO_2 k_H by 17-37% and underestimates that of N_2 by 20-30% being considered a good agreement [10]. The experimental data fall within the range predicted by the MD simulations.

Table 8. Henry's constants ($cm^3kg^{-1}MPa^{-1}$) for CO_2 and N_2 in PP measured at 461K [9]. In the present study (MSC) the limits for k_H corresponding to a 95% confidence interval are calculated from an MD trajectory at 453.2 K. From Sanchez-Lacombe type equations [10], k_H at 461K and 453K are calculated.

	k_H (CO_2)	k_H (N_2)
Durrill&Griskey [9] 461K	2250±180	1310±110
Sato *et al.* [10]		
461 K	2830	971
453 K	2729	921
MSC (453K)	(1630< k_H ≤2570)	(737< k_H ≤1063)

The limits of the confidence interval of k_H calculated from NPT-MD are determined by the dynamic fluctuations of the unit cell total volume (Figure 8) and the amount and distribution of void space (Figure 8, inset).

However, for a more conclusive validation, NPT-MD trajectories for the PP matrix were calculated for a range of temperatures between

[3] The critical temperatures for CO_2 and N_2 are 304.1K and 126.2K, respectively [11].

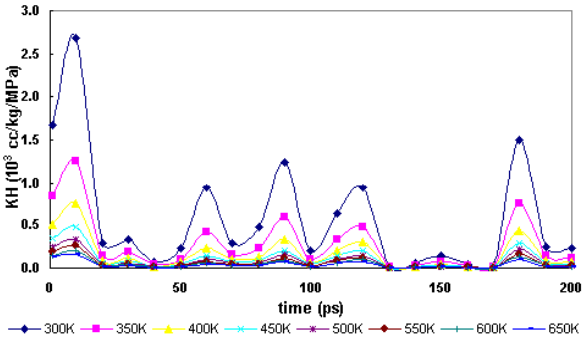

Figure 15. Time fluctuations of Henry's constant over a dynamic trajectory for which the PP is kept at 300K while the temperature of the N_2 molecules range from 300K and 650K.

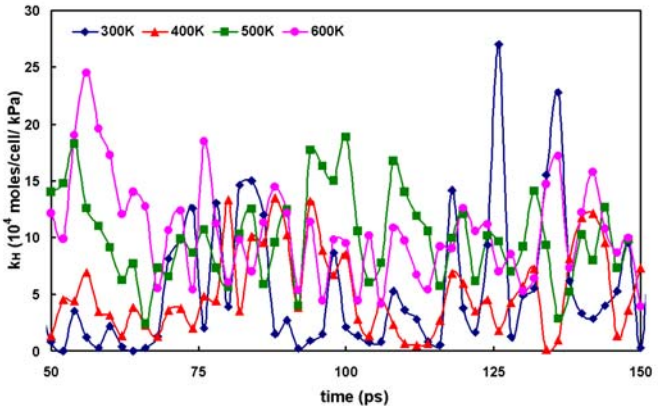

Figure 16. Time fluctuations of Henry's constant of N_2 for four temperatures where the dynamics of the polymer (PP) matrix at that temperature was considered.

300 K and 650 K (steps of 50 K) to study the temperature dependence of k_H of N_2 and CO_2 for this polymer. Henry's constant, k_H, was calculated using the ensemble method described in section 3 for frames every 2 ps along the equilibrated 100 ps MD trajectory. This temperature range covers both the glass transition temperature of PP (280K) and the melting temperature of 100% crystalline PP (~459K).

Temperature influences both the dynamics of the polymer matrix and that of the solute. This leads to changes in the solute-polymer interactions and makes Henry's constant temperature-dependent. To extract each of these effects separately and obtain their influence on the fluctuations of the system, two sets of calculations are performed. First, we considered the dynamics of the polymer matrix at 300 K and calculate Henry's constant for the 300 K - 650K temperature range (the matrix is maintained at a constant temperature and only the solute is heated). Second we included the temperature dependence of the polymer dynamics (both polymer matrix and solute are heated simultaneously). According to Equation 7, the first case should lead to values of k_H that scale inversely proportional with temperature as shown in Figure 15 while the behavior with time will be the same. Since the polymer dynamics is for 300 K, the temperature dependence of Henry's constant includes only the variation with temperature of the interaction energies of the gas-polymer system. Both N_2 and CO_2 lead to the same trend (data for CO_2 are not shown).

By including the temperature dependence of the polymer matrix in the calculations of k_H, two contributions to Eq. 7 will be affected: V_{cell} and U(r, Θ).

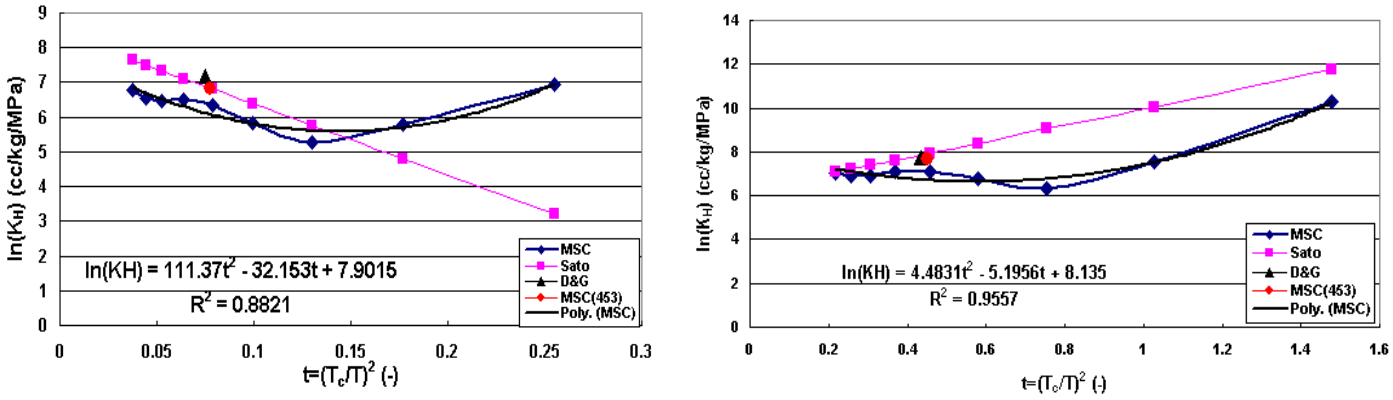

Figure 17. Ln(k_H) calculated in the present study (MSC) as function of the reduced temperature, t, for the case of N_2 (left) and CO_2 (right) in PP. A second order polynomial was fitted through the data points. Data from [19] using a Sanchez Lacombe equation of state are plotted. Values from Table 5 are also added to the graph

Especially at temperatures close and above the melting temperature (T_{melt}) of the polymer, the total unit cell volume exhibits larger fluctuations (Figure 8). The solute-polymer interaction energy, U(r, Θ), determined by the "chemistry" of the internal surface of the pores will also change as the polymer chains will have an increased chance to modify their configurations. The overall effect on the temperature dependence of Henry's constant is thus including both these effects (Figure 16).

Stern et al. [19] proposed to use a linear expression between k_H (cc (STP)/kg MPa) and the reduced temperature $t=(T_c/T)^2$ to correlate the data also used in the study by Sato *et al.* [10]. The critical temperatures, T_c, (304.1K for CO_2 and 126.2K for N_2) are obtained from Reid *et al.* [11]. Eq. 10 was thus used to compare the k_H values determined in the present study (denoted by MSC) for N_2 and CO_2 in PP (Figure 17), with existing literature studies [9, 10]. Sato's data are calculated by extrapolating Eq. 10 for a range of temperatures between 250K and 650K (the corresponding range for the reduced temperature, t, is approximately 0.25 to 0.04 for N_2 and 1.5 to 0.21 for CO_2). The value determined by Durrill & Griskey [9] at 461K is also added to Figure 17 together with the additional calculation at 453K by MSC (also compared in Table 8).

There is a clear discrepancy at low temperatures (large t) for nitrogen in PP between our calculations and Sato's data. While our data show that there is a distinct minimum at a temperature of about 350K, Sato's equation suggests a linear dependence. This is most probable related to the fact that in Sato's experimental study the amount of data was not sufficient to obtain a definite temperature dependence of Henry's constant. One study reported by Sato [10] suggests that usually the glass transition temperature for the polymer matrix is also the temperature of minimal

solubility for *noble* gases. This behavior is based on measurements of a series of noble gases in poly(methylacrylate) and could be explained by the contribution to Henry's constant from filling the voids in the polymer matrix. A comparable result is determined by Sato for N_2 in poly(styrene). The glass transition temperature of isotactic poly(propylene) is 373K that corresponds to a reduced temperature of t=0.11. Both the overall trend for the temperature dependence of k_H for N_2 in PP and the temperature of minimal solubility predicted in this study are in very good agreement with the above suggested noble gas behavior.

For carbon dioxide + PP the presence of a minimum is less pronounced and also occurs at higher temperatures (t=0.8) than for nitrogen. As suggested by Sato [10], there are two competing effects. At low temperatures the gas condensation dominates while at higher temperatures the solute-solvent mixing becomes important. As the critical temperature for CO_2 is higher than for N_2, the gas condensation is also more important. Over the same temperature range, Henry's constants for carbon dioxide in PP are larger than those of nitrogen, the difference being (2-5 times larger at temperatures below the melting temperature of PP) decreasing with increasing temperature.

Figure 17 shows that our calculations are consistent with Henry's constant temperature dependence predicted in other literature studies. This consistency gives some confidence in the integrity of our calculations.

5 Results and discussion

The solubilities of oxygen and water vapor in PET, PVOH, PVDC and PP at a temperature of 300 K are summarized in Table 9 and Table 10, respectively. Henry's constant values are calculated according to the methodology described in section 3. Following the procedure described in section 2, the polymer samples are generated and selected for a 200 ps molecular dynamics trajectory. To be noted that the calculations for water vapor include electrostatic interactions whereas those for oxygen do not.

Table 9. Solubility constants of oxygen in PVOH, PET, PP and PVDC (ordered from least to highest soluble). The interval of variation for Henry's constant, k_H, is calculated for a 95% confidence level.

Polymer	ρ_{exp}	k_H	k_H
-	g/cc	molec/cell^{-1}/kPa^{-1}	cm^3/cm^3/atm
PVOH	1.29	(5.2<μ≤6.4)*1e-4	(0.41<μ≤0.50)
PET	1.34	(6.2<μ≤9.2)*1e-4	(0.46<μ≤0.68)
PP	0.86	(1.0<μ≤1.4)*1e-3	(0.53<μ≤0.74)
PVDC	1.66	(1.7<μ≤2.1)*1e-3	(0.75<μ≤0.92)

Table 10. Solubility constants for water vapor in PP, PVDC, PET and PVOH (ordered from least to highest soluble). The interval of variation for Henry's constant, k_H, is calculated for a 95% confidence level.

Polymer	ρ_{exp}	k_H	k_H
-	g/cc	molec/cell^{1}/kPa^{1}	cm^3/cm^3/atm
PP	0.86	(2.4<μ≤4.2)*1e-4	(0.13<μ<0.22)
PVDC	1.66	(1.4<μ≤2.2)*1e-2	(6.5<μ<10.2)
PET	1.34	(1.3<μ≤2.9)*1e-1	(96<μ<214)
PVOH	1.29	(0.3<μ≤1.3)	(235<μ<1017)

According to Figure 1, the most oxygen **permeable** membrane of the four investigated

here is PP followed by PET, PVOH and PVDC. Except for the case of PVDC, the hierarchy is preserved also from the solubility point of view (Table 9). The present calculations predict that PVDC is the highest oxygen soluble membrane of the investigated four. The oxygen solubilities of these four polymers differ only by a factor of 2 while the difference in permeabilities is about four of orders of magnitude between the highest and least permeable.

For water, the most **permeable** membrane is PVOH followed by PET, PP and PVDC (Figure 1). This hierarchy is again preserved also for the case of solubility except that PVDC is more soluble to water than PP. That PVOH has the highest solubility for water is most probable explained by the presence of hydrogen bonds between the terminal OH groups (Figure 2) and water molecules. Some hydrogen bonds may also be present in the case of PET between the backbone or side oxygen atoms and water molecules (Figure 2). Compared to the case of oxygen, water solubilities differ by a larger amount (four orders of magnitude) and so do the corresponding permeabilities. It may thus be that in the overall permeability properties of a membrane towards water solubility plays a more important role than for the case of oxygen.

Other factors like polymer crystallinity, tacticity, orientation and cross-linking certainly influence the permeability properties of the formed membrane. For example, polymers characterized by a high degree of crystallinity normally exhibit lower permeabilities. Recently it has been shown experimentally that some clay/polymer composites may offer significantly reduced permeabilities over the individual polymer materials. This can be explained partly by the added tortuosity of the path that a gas molecule or atom must take to transverse the polymeric nanocomposite membrane due to the combination of crystalline and amorphous regions.

Table 11. Average values of total volume, densities and Henry's constant for the minimized polymer samples generated with the CED procedure.

Polymer	V_{cell}	Density	k_H
	$Å^3$	g/cc	molec/cell/kPa
PCTFE	(8658±335)	(1.79±0.07)	(1.0<μ≤1.9)*1e-3
PP	(6879±189)	(0.81±0.02)	(1.6<μ≤5.8)*1e-4
PVOH	(4857±89)	(1.21±0.02)	(0.1<μ≤4.9)*1e-4
PVDC	(8233±116)	(1.56±0.02)	(1.1<μ≤2.1)*1e-3
PET	(4888±88)	(1.31±0.02)	(0.1<μ≤4.8)*1e-4

Although higher density polymers should in principle exhibit lower solubilities, the present study performed on low molecular weight samples does not seem to exhibit such a trend. For the four investigated samples, oxygen and water solubilities do not decrease with increasing density (Table 9-10). A similar result is obtained if Henry's constants are calculated from CED generated samples (Table 11).

The confidence limits for MD-calculated Henry's constants are relatively large. As discussed in section 4 for the validation case of nitrogen and carbon dioxide in PP, the source of these large fluctuations is caused by the thermal fluctuations in the polymer matrix (total volume of the unit cell) during the molecular dynamics run. Figure 12 shows such a variation for the PP sample and may be considered representative for the dynamics of all the polymers investigated in the present study. A second cause for the spikes observed in the temporal variations of Henry's constant (Figure 15 and Figure 16) is the "chemistry" of the internal surface of the pores described by the solute-polymer interaction energy, $U(r, \Theta)$, which also changes whenever the polymer chains modify their configurations.

Other factors, such as the presence of the polymer terminal ends and the duration of the MD simulation from which Henry's constant is calculated, could also be a cause for the observed fluctuations. The effect of such factors on the limits of the confidence level of Henry's constant in separately investigated below for the case of oxygen solubility.

It is conceivable that the fluctuations in Henry's constant might be related to some specific feature of the chemical structure of the investigated polymers. Thus systems like PP, PVOH and PVDC that do not contain aromatic rings explore probable more easily a larger number of conformations, allowing "bad configurations" to be eliminated during the dynamics simulation. However, data in Table 9 and Table 10 do not seem to indicate that such an effect exists, the confidence interval for PET being comparable with that of other polymers.

Terminal ends of the polymer chains could also influence the dynamics and thus, the confidence interval determined for k_H. An infinite molecular weight chain of PET is constructed by building many times the polymer unit cell for finite chains. When terminal groups are located close to each other, they are connected. From 200 ps of MD at 300K, oxygen Henry's constant is found to be $(5.8<\mu\leq 8.0)$*1e-4 molecules*cell^{-1}*kPa^{-1}, with a confidence interval for k_H about 40%, comparable with that in Table 9.

Although a detailed study of the temperature dependence of Henry's constant of nitrogen and carbon dioxide was performed for the case of poly(propylene), the effect of high temperatures (1000 K) on the confidence interval with which Henry's constant is determined was tested once more. A 200 ps molecular dynamics trajectory for the PET sample is generated at 1000 K. Oxygen Henry's constant is determined as $(5.9<\mu\leq 8.5)$*1e-6 molecules*cell^{-1}*kPa^{-1}. Compared to the confidence interval at 300K, $(6.2<\mu\leq 9.2)$*1e-4 molecules*cell^{-1}*kPa^{-1}, a decrease by two orders of magnitude in the average value of Henry's constant is observed

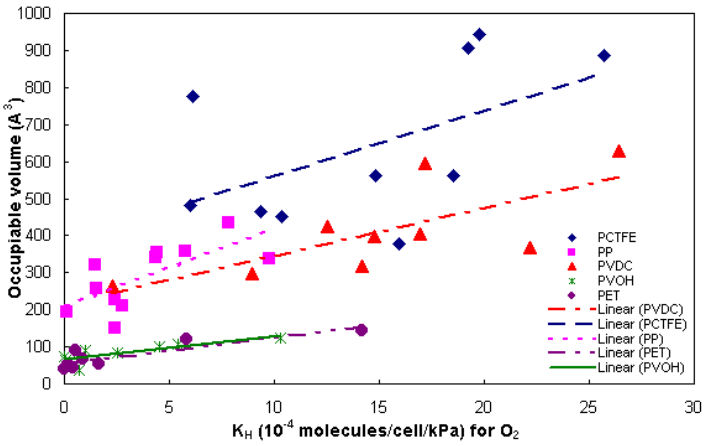

Figure 18. Correlation between Henry's constant values for oxygen and the occupiable volume in the polymer matrix for the minimized samples generated with the anneal dynamics procedure. The probe radius in the calculation of occupiable volume was 1.2Å. R^2 values are 0.2 for PCTFE, 0.5 for PP and PVDC, 0.6 for PVOH and 0.7 for PET.

but the width of the confidence interval remains comparable (~45%).

As polymeric systems might require longer equilibration periods, the effect of a longer MD simulation (400 ps instead of 200 ps for the PET sample) on the confidence interval calculated for Henry's constant is investigated next. The confidence interval for oxygen solubility in PET calculated for the 20-400 ps interval from the 400 ps MD run (n=76) is $(5.6<\mu\leq 6.5)$*1e-4 molecules*cell^{-1}*kPa^{-1}. This value is significantly reduced from ~60% to ~20% and suggests that for more accurate determinations the polymer samples should be equilibrated for longer time periods.

Experimental investigations show that - especially for highly soluble and dense gases- the quantity of dissolved gas can be appreciable and usually leads to polymer swelling. Naturally in such cases, a correlation between Henry's constant and the total and/or occupiable volume[4] characteristic for the modeled polymer samples could exist. Henry's constants calculated via the Henry's constant ensemble are plot as a function of the occupiable volume for the five polymer samples. However, for none of the polymers a clear correlation could be established (data not shown). Similar correlations between the occupiable volume and Henry's constant values were sought for the minimized samples generated with the CED procedure (Figure 18). PP, PVDC and PCTFE (R^2 values of 0.5, 0.5 and 0.2) show good correlations while PET and PVOH do not (R^2 values of 0.7 and 0.6).

An additional test was set where PET samples (10 chains with degree of polymerization 5) are built with the same total volume of the unit cell (V_{UC}=1311 Å^3) using the Amorphous Builder module of Cerius^2 (Accelrys Inc.). The "void" distribution of the polymer sample is controlled by including during the building process:

1. *no* oxygen molecules;
2. *one* cluster containing **ten** oxygen molecules;
3. *two* clusters, each with **five** oxygen molecules;

[4] The occupiable volume is the fraction of the total volume of the unit cell that can be occupied by a probe of radius R_p (includes isolated voids in the polymer matrix). A probe radius of 1.2 Å was used in the present study.

4. *ten* clusters each containing **one** oxygen molecule.

Prior to calculate Henry's constant, each of the above samples is minimized and the oxygen molecules removed. Henry's constant values are summarized in Table 12.

Table 12. Henry's constant for oxygen in PET with "controlled" occupiable volumes, V_{oc}, and void distributions for the same total volume of the unit cell, V_{UC}=1311 Å^3. The surface accessible area of the unit cell, S_C, and the surface area corresponding to the occupiable volume, S_{oc}, are also calculated

Sample	S_C	V_{oc}	S_{oc}	k_H
	Å^2	Å^3	Å^2	molec/cell/kPa
No O_2	1367	293	370	5.5e-3
1x10 O_2	2032	398	507	4.5e-3
2x5 O_2	1975	472	630	4.5e-3
10x1 O_2	1745	354	431	2.7e-2

When no oxygen molecules are included in the amorphous building procedure (case 1) the cell will contain the smallest amount of occupiable volume. Henry's constant also has the smallest value. Between the case of a single large void (case 2, k_H=2.7*e-2 molecules/cell/kPa) and ten small isolated voids (case 3, k_H=4.5*e-3 molecules/cell/kPa) the occupiable volume (and the corresponding surface area) is decreased by 11% but Henry's constant is larger by a factor of 6, contrary to what one might expect if a correlation would exist. Between one void with ten oxygen molecules (case 2) and two voids each containing five oxygen molecules, the occupiable volume is increased by ~19%. However, Henry's constant calculation in these two cases gives the same value.

Henry's constant value peaks however for case 4 where ten small "voids" are included in the structure, although the corresponding occupiable volume is not the largest.

Table 13. Henry's constant confidence intervals for oxygen in PET for two sample sizes, n=10 and n=100 and from trajectory averaging.

n	k_H (molec/cell/kPa)
10	(0.1<μ≤4.8)*1e-4
100	(4.5<μ≤6.4)*1e-4
Trajectory	(6.2<μ≤9.2)*1e-4

To test if ensemble average is more rigorous than trajectory (time) average, Henry's constant confidence levels are calculated for the minimized samples (n=10) generated with the CED procedure (Table 13). However it turns out that the confidence intervals determined as ensemble average are much larger than those obtained from average trajectory calculations (Table 9-10). This is certainly the case for calculations performed on small sets of polymer samples (n=10). The calculations are also repeated for the larger set n=100 generated for PET. The three calculated confidence intervals differ significantly although a slight overlap exists.

Most probably, by generating a larger set of samples for each polymer and determine Henry's constant for the minimized structures or alternatively calculate solubility via the Henry's

constant ensemble method for longer equilibrated polymers would lead to a more accurate value.

Table 14. Henry's constant, k_H, for oxygen in PET for frames with average, minimum, and maximum volume as selected from the trajectory or scaled (using fractional coordinates) from the initial frame at t=0.

V	V_{occ}	k_H	Observations
Å^3	Å^3	molec/cell/kPa	
4882.2	43.1	6.3e-6	Frame at190 ps
"	79.9	3.4e-4	Frame at t=0, scaled
"	65.9	7.6e-5	Frame at t=0, scaled and minimized
4729.2	23.9	1.7e-7	Frame at129 ps
4724.6	68.0	3.7e-4	Frame at t=0, scaled
4724.6	47.2	1.6e-5	Frame at t=0, scaled and minimized
5187.5	130.6	3.1e-4	Frame at 2 ps
5182.2	110.4	3.1e-4	Frame at t=0, scaled
5182.2	118.1	3.1e-4	Frame at t=0, scaled and minimized

During MD a certain region of the phase space is explored, thus favorable and unfavorable polymer conformations –defined from the point of view of the interactions with the solute- are sampled. To study the effect of such conformational changes on Henry's constants, frames are extracted from the PET trajectory at 300 K corresponding to average (4882.2±74.9 Å^3), minimum (4724.3 Å^3) and maximum (5182.1 Å^3) volumes. Additionally, the volume of the initial frame (t=0) is successively changed (using fractional coordinates) to the average, minimum and maximum dynamics volume. The volume-scaled initial frames are also energy minimized. Henry's constant is then calculated for each of these frames in the three listed cases.

For approximately the same average, minimum and maximum values of the unit cell volume, initial polymer conformations as generated from the CED procedure or as generated during molecular dynamics, result in significantly different values of Henry's constant (Table 14).

For example, by scaling the volume of the initial time frame to the average value, Henry's constant is a factor of ~5 smaller if the structure is also energy minimized.

Henry's constant calculated for the trajectory frame that has a volume closest to the average dynamics volume (frame at 190 ps) is another factor of ~13 smaller. Similarly, when the initial frame volume is scaled to the minimum dynamics value, Henry's constant increases only to decrease again after the structure is energy minimized.

6 Summary

The present study describes a combined molecular dynamics and Monte Carlo methodology to estimate *solubility properties* of polymeric membranes (PP, PET, PVDC, PVOH, PCTFE) with respect to a variety of solutes (nitrogen, carbon dioxide, oxygen and water). Solubility (Henry's constant) is only one property that defines the overall permeability of a polymeric membrane. However, it seems that solubility for water is more important than for

oxygen in defining permeability, probably due to its hydrogen binding potential and electrostatic interactions.

Although this study uses samples of amorphous polymers with low molecular weights and relative short molecular dynamics runs (200 ps) compared to the time scale at which the whole process of permeation (diffusion and sorption) occurs it provides a useful and relative quick tool to better understand the process of gas solubility in polymeric matrices. The correct trend is predicted for the variation of Henry's constant with temperature of nitrogen and carbon dioxide in poly(propylene), for temperatures below and above the polymer's melting point. Especially for noble gases the present method correctly predicted the temperature of minimal solubility, close to the glass transition temperature of the polymer.

For statistical accuracy, a confidence interval rather than an average value is calculated for Henry's constant, k_H. Also, to best capture structural variations characteristic to each polymer, a set of ten samples was generated. Ideally, the larger the sample set, the higher the accuracy of the calculated properties. Although the ten-sample set seems to be biased towards configurations with higher energies, it may still be considered representative. A good criterion to choose a sample from the generated set is on basis of average density and CED.

The relatively large intervals determined for Henry's constants are the result of a combination of various factors: sample equilibration and dynamics, total occupiable volume, size of voids and distribution, interaction energy solute-polymer matrix determined by "favorable" or "non-favorable" exposed surface of the polymer chains. Longer equilibrations of the polymer matrix and also energy minimization of the structure before calculating Henry's constant would certainly benefit the accuracy. However, these wide intervals have to be regarded as a characteristic of each polymer, directly related to its structural properties and the nature of its interactions with the solute.

Acknowledgements

This work was supported in part by a grant from the Avery Dennison Corporation. The facilities of the MSC were partly funded by NSF, DOE-ASCI, Chevron, NIH, ONR, Seiko-Epson, Kellogg's, General Motors, Beckman Institute, Asahi Chemical and Nippon Steel.

References

1. Seiichi Kashilara, Mihail Iotov, Siddharth Dasgupta, Guanghua Gao, Michael Belmares, and William A. Goddard III, in preparation.
2. Permeability and other film properties of plastic and elastomers, Plastic Design Library, Norwich, NY, 1995
3. N. Metropolis, A. W. Rosenbluth, M. N. Rosenbluth, A. N. Teller, and E. Teller, J. Chem. Phys., **21**, 1087 (1953).
4. Polymer Handbook (4th edition), ed. By J. Brandrup, E. H. Immergut, E. A. Grulke, John Wiley & Sons, Inc., 1999.
5. Cerius2 Property Prediction, ***, MSI manual, April, 1997
6. Allen, M. P, Tildesley, D. J, Computer simulation of liquids, Clarendon Press, Oxford, 1987.
7. Bezus, A. G.; Kiselev, A.V.; Lppatkin, A.A.; Pham Quang Du, J. Chem. Soc. Faraday Trans., 2, 74, 367, (1978)
8. Mayo, S. L, Olafson, B. D. and Goddard III, W. A., DREIDING: A Generic Force Field for Molecular Simulations , J. Phys. Chem. **94**, 8897 (1990)
9. Durill, P. L. and Griskey, R. G, Diffusion and solution of gases in thermally softened or molten polymers, A. I. Ch. Journal, 12(6):1147-1151, 1966.
10. Sato, Y., Solubilities and diffusion coefficients of carbon dioxide and nitrogen in polypropylene, high-density polyethylene and polystyrene under high pressure and temperature, Fluid Phase Equilibria, 162:261-276, 1999.
11. Reid, R.C. et all, The properties of gases and liquids, 4th Edition, McGraw-Hill, NY 1987, pp. 656.
12. ***, Permeability and other film properties of plastics and elastomers, Plastic Design Library, 1995.
13. M. Blanco, M. Belmares, R. B. Ross, S. H. Chou, T. Pham, P. Olafson, , C. Thomas and W.A. Goddard III; Hildebrand and Hansen Solubility Parameter from Molecular Dynamics, Submitted to Macromolecules.
14. Stanett, V.T. et all, Advances in Polymer Sciences, 32:69-121, 1978.
15. Vasile, C., Handbook of polyolefins, New York: Marcel Dekker, 2000.
16. Barton, Allan F. M., CRC handbook of polymer-liquid interaction parameters and solubility parameters, CRC Press, 1990.
17. P. Supaphol, J. E. Spuiell and J. S. Lin, Isothermal melt crystallization and melting behaviour of syndiotactic polypropylene, Polym Int, 49:1473-1482, 2000.
18. F. Muller-Plathe, Calculation of the free energy for gas absorption in amorphous polypropylene, Macromolecules, 24:6475-6479, 1991
19. S. A Stern, J. T. Mullhaupt and P. J. Gareis, AIChE J, 15, 64-73, 1969
20.

Appendix

This section summarizes the Rotational Isomeric State (RIS) tables and the charges on the five polymer samples (PET, PP, PCTFE, PVDC and PVOH) selected for the present solubility study. The RIS table contains information on the conditional probability of key dihedral angles in the polymer chain determined by separately minimizing the energy of the representative torsions, with coupling where applicable. The charges on the polymers are calculated from electrostatic potential fits (ESP) to Hartree Fock (6-31G** basis set) quantum charges using the Jaguar program (Schrödinger LLC). The atomic charges for the monomer structures are calculated first after replacing the head and tail atoms (hydrogens) by methyl groups (CH_3) to avoid terminal edge effects on the charges. A macro was then used to assign the Jaguar calculated quantum charges back to the monomer after first replacing the terminal methyl groups with hydrogen atoms. The residual charge was redistributed over the entire monomer, except for the terminal hydrogen atoms that remained uncharged. The terminal hydrogens are used as dummy atoms for the monomer as they are deleted when a polymer chain is generated. The monomer configuration with ESP charges was used to build a trimer and to determine the main representative torsions of the PET polymer.

1. Polyethylene terephtalate (PET)

The structure of the PET monomer (Figure 2) was loaded from the Cerius[2] (Accelrys Inc.) database. By including only main backbone atoms (side chains are easily realigned by dynamics), three representative torsions were selected. The torsions were denoted as t_1 (all $C\_3-O\_R-C\_3-C\_R$ type), t_2 (all $C\_3-O\_R-C\_3-C\_3$ type) and t_3 (all $O\_R-C\_3-C\_3-O\_R$ type), respectively. To optimize the polymer geometry by calculating the torsional potentials and the Rotation Isomeric Structure (RIS) table, torsion t_1 was minimized first. Torsions t_2 and t_3 were then minimized after coupling with t_1, and t_2, respectively.

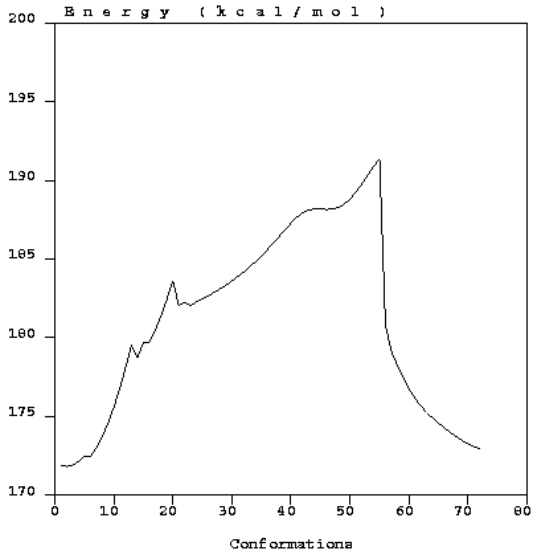

Figure 19. Energy (kcal/mol) as function of the total number of conformation for torsion t_1 (all atoms with C_3-O_R-C_3-C_R type) of PET.

For torsion t_1, the energy variation as a function of the total number of conformations of the trimer (Figure 19) indicates the presence of three local minima of the energy, each corresponding to a representative state of the polymer. Table 15 summarizes the angle values and their tolerances that correspond to these local minima in the energy.

Table 15. Angles and energies characterizing the three representative t_1 states of PET.

Angle (deg)	Tolerance (deg)	Energy (kcal mol^{-1})
45.0	10.0	188.2
185.0	10.0	171.8
290.0	10.0	182.1

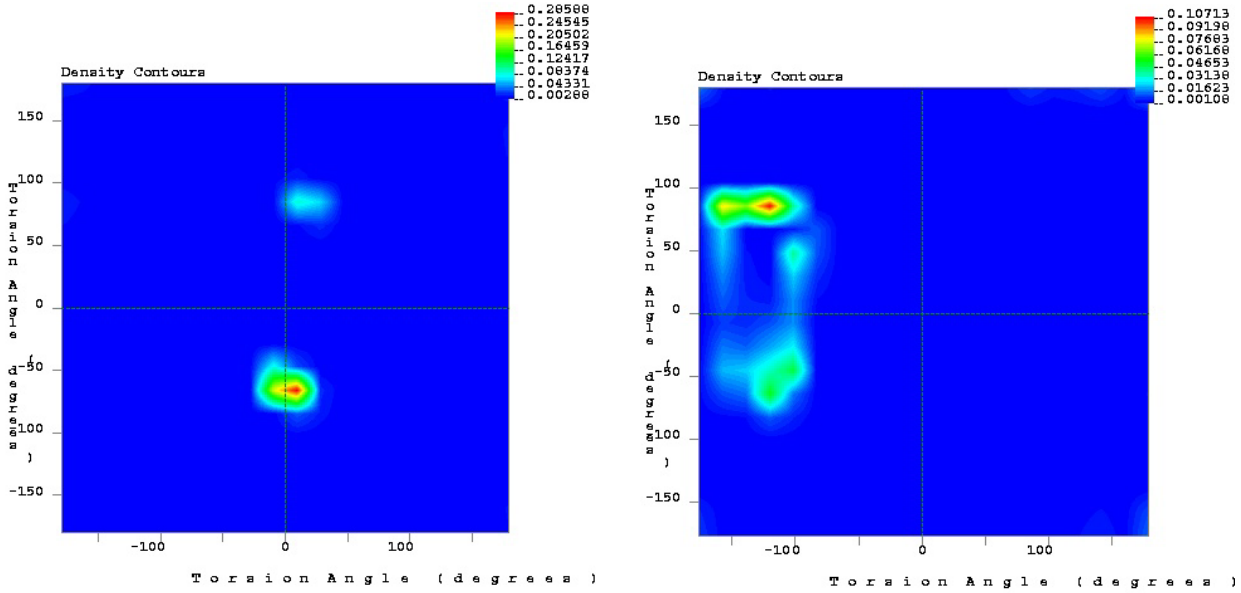

Figure 20. Density contours for coupled torsions t1-t2 and t2-t3 in PET. Dark blue regions correspond to low correlated torsions (low energies) while the correlation degree increases the brighter the color.

For the analysis of the coupled t_1-t_2 and t_2-t_3 torsions, density contours are analyzed (Figure 20). The dark blue regions correspond to a low probability (low energy) of correlation angles. The degree of correlation increases with color brightening. Figure 20 indicates the existence of two local minima for the t_2 torsion (Table 16). The presence of the double bonded oxygen in the close vicinity of the resonant carbon makes it difficult for the structure to bend or flex. It seems that the optimal conformation occurs when the double bonded oxygen and the carbon-carbon resonant bond remain in the same plane.

Table 16. Representative states for coupled t_1-t_2 torsions.

T1\T2 deg	Δt_2 deg	29.0	14.3
74.9	25.0	161.0	155.0
275.0	30.0	155.0	151.6

Compared to the t_1-t_2 coupling, the t_2-t_3 coupled torsion has a higher number of states (Table 17) most probably because none of the two component torsions contains a resonant carbon that would restrain the structural freedom.

The RIS table was built by compiling Tables 15-17 and thus contains all the key information characterizing the representative states of equilibrium (or local equilibrium) of the polymer. For all three investigated cases (t_1, t_1-t_2, t_2-t_3) the given tolerances for the angles actually represent the range of variation that corresponds to a change in energy of 1%.

Table 17. Representative states for coupled t_2-t_3 torsions.

T3/T2 deg	Δt_3 deg	207.0	248.0	264.0
34.0	20.0	200.0	200.0	150.3
66.0	10.0	149.5	149.3	200.0
294.0	10.0	200.0	150.6	200.0
309.0	5.0	150.8	200.0	200.0

The RIS table is used as input for the CED procedure (section 2, [13]) in which amorphous samples of a three dimensional periodic unit cell of the polymer are constructed.

The charges for the PET monomer and trimer are summarized in (Table 18).

Table 18. Atomic charges of the PET monomer.

Atom	Charge in monomer	Charge in trimer (ESP)
C1	0.65606	0.66205
C2	-0.12530	-0.11931
H3	0.13972	0.14571
C4	-0.15101	-0.14502
H5	0.13896	0.14495
C6	-0.08504	-0.07905
C7	-0.10243	-0.09644
H8	0.14725	0.15324
C9	-0.11571	-0.10972
H10	0.13693	0.14292
C11	-0.09128	-0.08529
O12	-0.55509	-0.54909
C13	0.77351	0.77950
O14	-0.46129	-0.45529
O16	-0.53615	-0.53016
C17	0.08063	0.08662
H18	0.09454	0.10053
H19	0.07788	0.08387
C20	0.21222	0.21821
H21	0.02388	0.02987
H22	0.04991	0.05590
O23	-0.44006	-0.43407

2. Polyvinylidene chloride (PVDC) and polyvinyl alcohol (PVOH)

Both polymers, PVDC and PVOH, have a representative torsion, t_1, defined by the backbone carbon atoms (C-C-C-C). The torsion energy distribution was determined for the dimer as it contains the minimum number of monomers for which this torsion is defined. The angles and energetic minima for PVDC and PVOH are summarized in Table 19.

The atomic charges for PVDC and PVOH are shown in Figure 21.

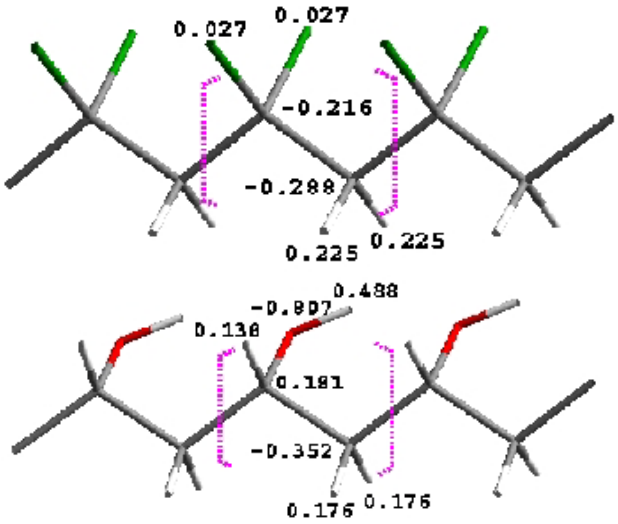

Figure 21. Atomic charges on PVDC (top) and PVOH (bottom) from quantum mechanics.

Table 19. Angles and energies characterizing the three representative t_1 states of PVDC.

Polymer	Angle (deg)	Tolerance (deg)	Energy (kcal mol^{-1})
PVDC	50.0	10.0	16.101
	85.0	10.0	18.918
	310.0	10.0	16.117
PVOH	50.0	20.0	1.054
	175.0	10.0	0.000
	260.0	12.0	4.088
	290.0	10.0	4.720

3. Polypropylene (PP)

The torsional potential (Figure 22) was determined via a grid scan (from -180^0 to 175^0 in steps of 5 degrees) on the middle torsion of the polypropylene pentamer and indicates a relatively rotatable bond. The energy difference between the lowest and highest energy conformers is about 10 kcal/mol.

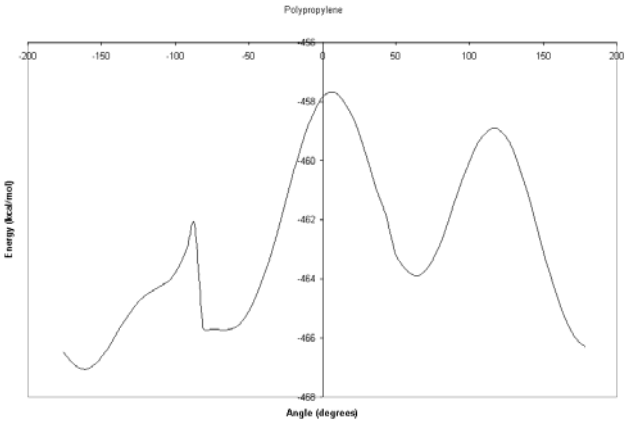

Figure 22. Torsional potential for the main torsion of PP.

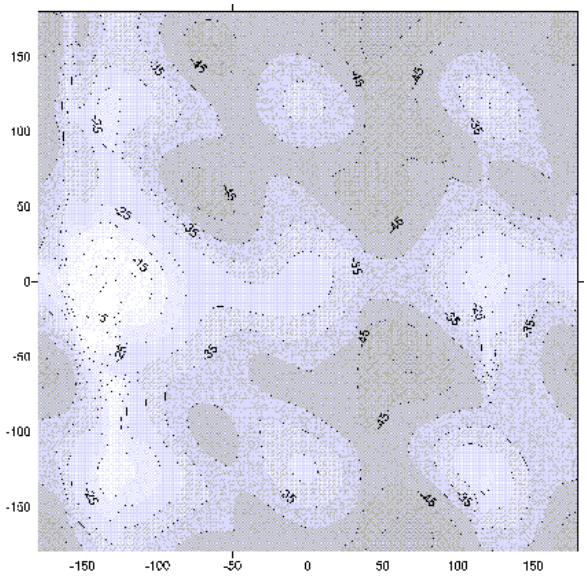

Figure 23. Torsional potential for the main torsion of PCTFE

From this potential plot, an RIS table (Table 20) was created and used to prepare the CED samples (syndiotactic PP 20-mer).

Table 20. Angles and energies characterizing the three representative t_1 states of PP.

Angle (deg)	Tolerance (deg)	Energy (kcal mol^{-1})
45.0	10.0	1.000
240.0	2.0	3.000
320.0	4.0	0.000

The atomic charges for the PP system were calculated using quantum mechanics (Table 21), then averaged out to create a neutral monomer that was repeated to generate the polypropylene polymer.

Table 21. Atomic charges of the PP monomer.

Atom	Charge in Monomer	Charge in Trimer
C (tail)	-0.5576	-0.55904
H	0.1304	0.12900
H	0.1035	0.10204
C (head)	0.5393	0.53785
H	-0.0549	-0.05636
C (methyl group)	-0.4961	-0.49754
H	0.1219	0.12044
H	0.1033	0.10192
H	0.1103	0.10890

4. Polychlorotrifluoroethylene (PCTFE)

PCTFE has a chiral center at the carbon bonded to both a chlorine and a fluorine atom. Because of this chiral center, tacticity had to be taken into consideration. Syndiotactic polymers were used for all calculations.

This polymer has two torsional angles that define it, and because there are two torsions, a coupled RIS table was generated. The dreidii-exp6-direct.par force field was used for the conformer search, done through a grid scan. Two torsions were varied, which resulted in 5,184 conformers (scanning angles from –180 to 175 degrees in 5 degree intervals). The most central torsion was used for both dihedrals. The corresponding Ramachandran plot is shown in Figure 23.

The RIS table for coupled torsions is slightly more complicated. A simple, uncoupled RIS energy table was generated for the first torsion (Table 22) and then a second table was coupled to the first (Table 23). The atomic charges of the PCTFE monomer and trimer are summarized in Table 24.

Table 22. Angles and energies characterizing the three representative t_1 states of PCTFE.

Angle (deg)	Tolerance (deg)	Energy (kcal mol^{-1})
0.0	5.0	4.000
120.0	5.0	4.000
230.0	10.0	0.000

Table 23. Representative states for coupled t_1-t_2 torsions of PCTFE.

T1\T2 deg	Δt_2 deg	0.0	120.0	230.0
0.0	15.0	4.000	4.000	0.000
130.0	3.0	4.500	4.500	0.500
232.0	5.0	4.750	4.750	0.750

Table 24. Atomic charges for the PCTFE monomer.

Atom	Charge in Monomer	Charge in Trimer
C (chiral center; attached to head)	-0.1887	-0.18360
Cl	0.0776	0.08271
F (attached to chiral center)	-0.0215	-0.01644
C (attached to tail)	0.4128	0.41789
F (labeled F13)	-0.1413	-0.13623
F (labeled F14)	-0.1390	-0.13392